Photoemission spectromicroscopy of neurons

Gelsomina De Stasio*
Istituto di Struttura della Materia del Consiglio Nazionale delle Ricerche, Via Enrico Fermi 38, Frascati, Roma, Italy

S. Hardcastle and S. F. Koranda
Department of Physics, University of Wisconsin–Milwaukee, Milwaukee, Wisconsin 53211

B. P. Tonner
Department of Physics, University of Wisconsin–Milwaukee, Milwaukee, Wisconsin 53211
and Synchrotron Radiation Center, University of Wisconsin, Madison, Wisconsin 53706

Delio Mercanti and M. Teresa Ciotti
Instituto di Neurobiologia del Consiglio Nazionale delle Ricerche, Viale Marx 15, 00100 Roma, Italy

P. Perfetti
Istituto di Struttura della Materia del Consiglio Nazionale delle Ricerche, Via Enrico Fermi 38, Frascati, Roma, Italy

G. Margaritondo
Institut de Physique Appliquée, Ecole Polytechnique Fédérale, PH-Ecublens, CH-1015 Lausanne, Switzerland
(Received 29 May 1992; revised manuscript received 26 October 1992)

We present photoemission spectromicroscopy results on biological specimens. The data, obtained with x-ray secondary (photoelectron) emission microscopy, study individual elements in micrometer-size portions of neuron networks.

PACS number(s): 87.80.+s, 07.80.+x, 79.60.−i

We present results of an experiment in the life sciences: photoemission chemical analysis on a microscopic scale [1]. A secondary-photoelectron microscope [2,3] was used to obtain microimages of several neuron networks with a lateral resolution of 0.5 μm. Then, the same instrument analyzed chemical elements and their status on the same microscopic scale. The test was performed on oxygen and on traces of two uptaken toxic elements, cobalt and manganese.

Photoemission spectroscopy has been for many years a leading probe of the chemical and electronic structure in materials science [1,4]. Unfortunately, its applications to biological systems have been drastically limited by insufficient lateral resolution. Recently, this obstacle has begun to be removed by dramatic improvements in the instrumentation [1–8]. High-quality secondary-photoelectron microimages of neuron networks have been obtained with resolution in the half-micrometer range, both with the electron-imaging instrument used in the present work [3] and with the scanning instrument MAXIMUM at Wisconsin [6]. Figure 1 shows an example of an electron-imaging secondary-photoelectron micrograph, revealing fine details of a neuron network.

The present work goes beyond the mere imaging, and performs tests of chemical analysis. The experiments were conducted on fixed and dehydrated neuron networks. Cerebellar granule cells from 7-d-old rats were allowed to grow on a gold substrate. The cells were obtained [9] by enzymatical and mechanical dissociation of the cerebellar tissue and plated at a density of 10^5 cells/cm^2 in Basal Medium (Eagle's salt), containing 10% fetal calf serum. Dissociated cells were seeded in Petri dishes on a gold-coated stainless-steel substrate, treated with a 5 μg/ml of poly-L-lysine solution, and cultured in an incubator at 37 °C in a 5% CO_2 humidified atmosphere.

Afterwards, we followed either one of two final procedures in the specimen preparation process. In the first procedure, after 6 d the cultures were fixed for 10 min in a 4% solution of para-formaldehyde in phosphate buffered saline solution (PBSS), carefully washed with distillated and deionized (DD) water, and dehydrated at a pressure of 10^{-3} mbar, at room temperature for 24 h [3,6].

The second procedure led to an uptake of toxic elements, either cobalt or manganese. The 8-d-old specimens were washed twice in an uptake buffer [10] to remove the culture medium, incubated for 20 min with $CoCl_2$ or $MnCl_2$ (5 mM in 1 ml of the same buffer) and in the presence of a neurotransmitter: 10 μM kainate of glutamate for cobalt uptake and 100 μM glutamate for manganese uptake. These neurotransmitters excite and swell the neurons and facilitate the penetration of toxic elements through the sodium and calcium membrane channels. Based on many tests performed with kainate and glutamate as well as with NMDA (*N*-Methyl-D-asparatate) and with no neurotransmitter, we confirmed the results of Ref. [11], that kainate is the most effective in enhancing the cobalt uptake.

Afterwards, the manganese-doped specimens were

twice washed in the uptake buffer and placed for 5 min in a solution of Na_2S plus NH_4Cl to induce precipitation of manganese sulfate (whose solubility is quite low), fixed for 10 min in para-formaldehyde (4% in PBSS), washed once in the uptake buffer and twice in DD water and dehydrated as in the first procedure. For cobalt-doped specimens, the double washing in the uptake buffer was followed instead by fixing for 10 min with para-formaldehyde in the presence of α-nitrose-β-napthol to induce precipitation of the toxic element, and then by washing and dehydratation.

The specimens doped with toxic elements were characterized with induced coupled-plasma (ICP) emission spectroscopy [12], after detaching the neurons from the substrate and suspending them in HNO_3. ICP is the most sensitive type of quantitative chemical analysis, capable of detecting elements in concentrations as low as 1 ppb. The ICP tests (see Ref. [11]) enabled us to prove the presence of the toxic elements in the neural cultures, demonstrating in particular the effectiveness of kainate in stimulating the Co uptake. The limit of ICP with respect to spectromicroscopy is, of course, the impossibility of studying space distributions.

The x-ray secondary (photoelectron) emission microscope (XSEM) used in the present study produces spatially resolved chemical information by measuring the secondary-photoelectron emission intensity as a function of the photon energy [1–3]. This requires using a tunable synchrotron-light source, in the present case the storage ring Aladdin at the Wisconsin Synchrotron Radiation Center, filtered by either a 10- or a 3-m toroidal grating monochromator. The XSEM, described in detail in Refs. [2] and [3], achieves high lateral resolution by means of an electron-optics system, including an objective lens to accelerate the electrons and form a first focused image of the emitting surface, a contrast aperture in the back-focal plane (diffraction plane) of the objective lens to define the accepted solid angle of electrons leaving the sample surface, a projective lens to provide additional, variable magnification, and a two-stage chevron micro-channel-plate electron multiplier array (CEMA) and phosphor screen assembly. Images formed on the phosphor screen are recorded using a TV camera with an 18-mm-diam silicon-target array low light-level vidicon tube—either at standard 30-Hz TV rates on magnetic tape, or digitized into frames of 512 horizontal by 480 vertical pixels using real-time image processing hardware in an 80386-based microcomputer.

Images like that of Fig. 1 are quite typical as far as overall quality and resolution are concerned. To perform

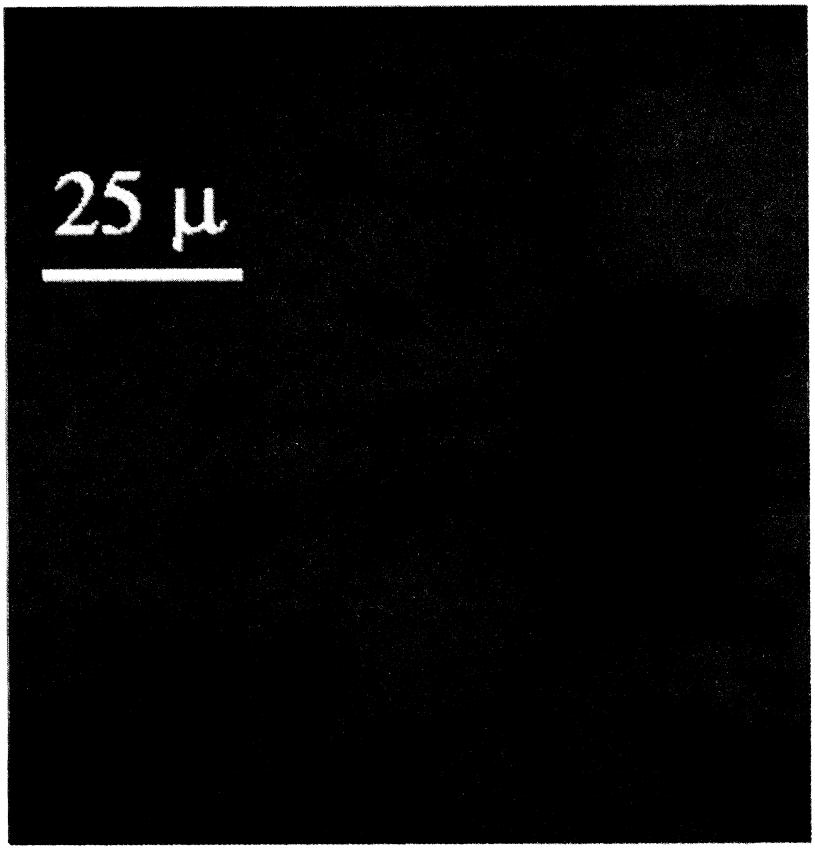

FIG. 1. XSEM secondary-photoelectron micrograph of a portion of neuron network of rat cultured cerebellar granule cells, taken with unmonochromated synchrotron light with a lateral resolution of the order of 0.5 μm. In the right-hand part of the image there is an aggregate of neurons, with several individual cells and their connections. In the central upper part, we see a growth cone.

chemical analysis, the XSEM can be used to measure the secondary-photoelectron emission intensity as a function of the photon energy from up to six selected microscopic areas of the sample simultaneously. The resulting spectra show high-resolution x-ray-absorption near-edge structure (XANES's), which reflect the chemical state of the analyzed region [13]. An example is show in Fig. 2 for specimens produced by the first procedure. We see the well-resolved bound-state and continuum resonances from oxygen [14] in two different areas selected from a bundle of fasciculated axon fibers (curves *b* and *c*). For comparison, the substrate region (curve *a*) has very little intensity in the oxygen-edge spectrum. In the latter case, the oxygen is most probably contained in the poly-*L*-lysine that covers the gold substrate.

The two principal spectral features are due to O $1s \rightarrow \pi^*$ transitions near 531 eV, and to a broader O$1s \rightarrow \sigma^*$ continuum resonance above the secondary-photoelectron emission threshold about 8 eV higher in energy [14]. The relative intensity and energy splitting between the π^* and σ^* resonances has been found to be correlated to the chemical state of oxygen in compounds, and in particular to the oxygen bond length [14]. Note that the quality of the spectra of Fig. 2 is largely sufficient to distinguish between the chemical status of oxygen in our specimen and that, for example, of chemisorbed O_2. The two spectral features in Fig. 2, curves *b* and *c*, are indeed centered at 532.2±0.5 and 539.(8)±1.5 eV; the corresponding values from Wurth *et al.* (Ref. [14]) are instead 530.0±0.5 and 536.5±1.0 eV for chemisorbed O_2, reflecting large and detectable differences in the chemical shifts.

A second typical example of microchemical analysis is shown in Fig. 3. Curves *b*, *c*, and *d* were all taken from 1×1 μm^2 areas of cobalt-doped neuron systems, whereas curve *a* is a reference spectrum from a Co wire. Curves *b* and *d* were taken on a specimen produced with exposure to kainate, and curve *c* from a specimen produced with exposure to glutamate. Both curves *b* and *c* were taken on axon areas, and curve *d* was taken on a cell body. Note that the shallow core-level edge Co3*p* is broader and has lower signal-to-noise ratio than the deeper O1*s* edge of Fig. 2.

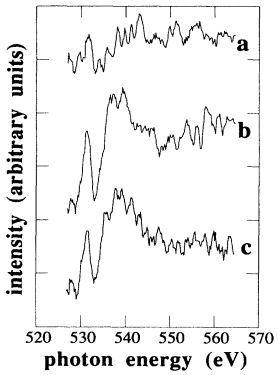

FIG. 2. Oxygen XSEM spectra [2] of a specimen without toxic elements, from three difference areas of approximately 2×2 μm^2: (a) from a substrate area; (b) and (c) from two different axon areas. The two typical optical absorption features of oxygen [13] can be observed at ≈531 and ≈538 eV. The data were normalized to the monochromator's output spectrum.

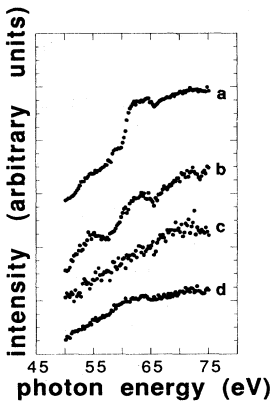

FIG. 3. Cobalt XSEM spectra of (a) a reference Co wire, and from three different 1×1 μm^2 areas of Co-doped specimens; (b) from an axon area and (d) from a cell body in a specimen treated with kainate; (c) from an axon area of a specimen treated with glutamate. The spectra were normalized to the same value for the lowest-energy point and then shifted with respect to each other for clarity. The analysis of the element distribution is discussed in the text.

The results of Fig. 3 demonstrate the presence of cobalt in at least some portions of the neuron specimen. A more quantitative assessment of the difference in cobalt concentration from place to place is possible under some general assumptions. If we take the ratio R between a cobalt spectral feature and the underlying background, its value is proportional to the cobalt content in the corresponding sample area, multiplied by the cobalt absorption coefficient, divided by the cumulative absorption coefficient of the other components of the sample, and multiplied by the ratio r of the absorbed-photon-to-electron-yield conversion factors for the cobalt absorption and for all other components. Assuming that all factors except the cobalt content are the same for different sample areas, the ratio of the R values for two different areas would reflect that of the cobalt contents.

Using the raw data, this would give a decrease in cobalt content of approximately a factor of ten between curve *b* and curve *c*—consistent with the independent evidence [11] for the superior effectiveness of kainate in stimulating cobalt uptake. Again using the raw data, the same hypotheses would give a change by approximately a factor of 2 in the cobalt content between curves *b* and *d*, reflecting possible inhomogeneities in the cobalt distribution.

Note, however, that the hypothesis on the invariance of r from place to place is quite strong, and may affect this last conclusion—which, therefore, must be taken with prudence. Possible variations of r are potentially due to several factors, and the volume of the emitting component of the neuron network appears the most critical. A systematic analysis of the r-factor effects is under-

way. We also note that, at present, we cannot distinguish between natural distribution inhomogeneities and possible effects of the specimen preparation procedure—in particular, effects of the precipitating agents.

In order to improve the reliability of our tests, we took spectra like those of Figs. 2 and 3 on different areas of different samples, specifically, cobalt-related spectra were taken on 20 different areas, always finding more Co-peak intensity on axons than on cell bodies. The data-taking time was of the order of minutes per spectrum.

We also found evidence for manganese signal in the Mn-doped samples. The experiments in this case were complicated by the volatility of the element, which made it difficult to correlate the XSEM signal intensity to the original distribution of the element.

A comprehensive comparison between the present technique and other methods of microchemical analysis suitable for biology is beyond the scope of this paper. We note, however, a remarkable complementarity between the XSEM microanalysis and techniques like scanning photoemission spectromicroscopy [5,6], energy-dispersive x-ray microanalysis [15], Auger microprobe, electron-energy-loss microanalysis [16], and laser microprobe mass analysis [17]. The complementarity primarily reflects the different capabilities of the corresponding non-space-resolved spectroscopies. In particular, photoemission techniques like the XSEM can better identify the chemical *status* of elements, reflected in the core-level chemical shifts—as we have seen in the case of Fig. 2. For example, the effective energy resolution of energy-loss techniques is more limited even with a reasonably high resolving power, because this last affects the absolute electron energy whereas the spectroscopic information is given by the (smaller) magnitude of the energy loss.

The energy resolution is also limited for other approaches [15,17]. Alternate techniques [15–17] have already reached higher spatial resolution than ours, but with primary-beam energy densities that are orders of magnitude higher than the XSEM, which worsens the damaging and charging problems.

The XSEM reaches indeed a space resolution better than 0.5 μm with a maximum power density of 10^{-10} W/μm^2, and a maximum energy density of 10^{-10} W/μm^2; this is, very conservatively, six–seven orders of magnitude better than a scanning electron microscope working at 0.1-μm resolution, and the comparison would become at least one order of magnitude more favorable for a microscope based on electron energy loss. Furthermore, the interaction phenomena are very different for electrons and photons, and in most cases these last are gentler probes because of their lack of mass and charge. In fact, extensive tests failed to provide evidence for primary-beam damage effects in the present experiments: such effects were only observed after very long exposure to an *unmonochromated* primary beam.

Sporadic charging effects were observed only when we used an unmonochromated photon beam, and then again after an exposure of several sec; such effects consisted of strong and increasing image deformations culminating in image instabilities and microsparks. These easily identified effects never occurred with monochromated beams, and do not affect the data discussed here.

Note that other techniques of photoelectron microanalysis [1,5,6] have high surface sensitivity and therefore are suitable for studying the cell membrane; the XSEM is not highly surface sensitive because of the low energy of the detected secondary photoelectrons. Such a low energy corresponds to a photoelectron escape depth ranging from hundreds to thousands of angstroms or more, i.e., to a probed region much thicker than the cell membrane.

In summary, the XSEM appears as a valuable and complementary augmentation of an important family of techniques for the microchemical analysis of biological specimens. In the present tests, we have shown that the XSEM can detect elements in neuron networks, and possibly reveal inhomogeneities in their distribution. We are currently extending this approach to other trace elements, to other sample preparation methods and notably to fast freezing, to other photon spectral ranges (which require different synchrotron beamlines) and to other photoemission experimental methods for microchemical analysis, notably [1,5,6] scanning photoelectron spectromicroscopy.

We are grateful to the ISA Italia and in particular to Dr. Oddo, Dr. Antonangeli, and Dr. Galli for giving us the possibility to perform the ICP tests. The expert help of Mario Capozi, Marino Marsi, Maddalena Pedio, and Tiziana Dell'Orto was essential to the success of the spectromicroscopy experiments. The work was supported by the Fonds National Suisse de la Recherche Scientifique, by the Consiglio Nazionale delle Ricerche, by the National Science Foundation and by the Ecole Polytechnique Fédérale de Lausanne. The spectromicroscopy experiments were performed at the Wisconsin Synchrotron Radiation Center, which is supported by the National Science Foundation.

*To whom correspondence should be addressed.

[1] For a recent review of photoelectron spectromicroscopy, see, for example G. Margaritondo and F. Cerrina, Nucl. Instrum. Methods A **291**, 26 (1990).

[2] B. P. Tonner, Nucl. Instrum. Methods **291**, 60 (1990).

[3] Gelsomina De Stasio, S. Koranda, G. Harp, B. Tonner, D. Mercanti, M. T. Ciotti, and G. Margaritondo (unpublished).

[4] G. Margaritondo, *Introduction to Synchrotron Radiation* (Oxford University, New York, 1988).

[5] F. Cerrina, B. Lai, C. Gong, A. Ray-Chaudhuri, G. Margaritondo, M. A. Green, H. Höchst, R. Cole, D. Crossley, S. Collier, J. Underwood, L. J. Brillson, and A. Franciosi, Rev. Sci. Instrum. **60**, 2249 (1989); F. Cerrina, S. Crossley, D. Crossley, C. Gong, J. Guo, R. Hansen, W. Ng, A. Ray-Chaudhuri, G. Margaridondo, J. H. Underwood, R.

Perera, and J. Kortright, J. Vac. Sci. Technol. A **8**, 2563 (1990); W. Ng, A. K. Ray-Chadhuri, R. K. Cole, S. Crossley, D. Crossley, C. Gong, M. Green, J. Guo, R. W. C. Hansen, F. Cerrina, G. Margaritondo, J. H. Underwood, J. Korthright, and R. C. C. Perera, Phys. Scr. **41**, 758 (1990); C. Capasso, A. K. Ray-Chaudhuri, W. Ng, S. Liang, R. K. Cole, J. Wallace, F. Cerrina, G. Margaritondo, J. H. Underwood, J. B. Kortright, and R. C. C. Perera, J. Vac. Sci. Technol. A **9**, 1248 (1991).

[6] Gelsomina De Stasio, W. Ng, A. K. Ray-Chaudhuri, R. K. Cole, Z. Y. Guo, J. Wallace, G. Margaritondo, F. Cerrina, J. Underwood, R. Perera, J. Kortright, Delio Mercanti, and M. Teresa Ciotti, Nucl. Instrum. Methods A **294**, 351 (1990); Delio Mercanti, Gelsomina De Stasio, M. Teresa Ciotti, C. Capasso, W. Ng, A. K. Ray-Chaudhuri, S. H. Liang, R. K. Cole, Z. Y. Guo, J. Wallace, G. Margaritondo, F. Cerrina, J. Underwood, R. Perera, and J. Kortright, J. Vac. Sci. Technol. A **9**, 1320 (1991); Gelsomina De Stasio, C. Capasso, W. Ng, A. K. Ray-Chaudhuri, S. H. Liang, R. K. Cole, Z. Y. Guo, J. Wallace, F. Cerrina, G. Margaritondo, J. Underwood, R. Perera, J. Kortright, Delio Mercanti, M. Teresa Ciotti, and Alessandro Stecchi, Europhysics Lett. **16**, 411 (1991).

[7] H. Ade, J. Kirz, S. Hulbert, E. Johnson, E. Anderson, and D. Kern, Nucl. Instrum. Methods **291**, 126 (1990).

[8] P. L. King, A Borg, C. Kim, P. Pianetta, I. Lindau, G. S. Knapp, M. Keenlyside, and R. Browning, Nucl. Instrum. Methods **291**, 19 (1990).

[9] G. Levi, F. Aloisi, M. T. Ciotti, and V. Gallo, Brain Res. **290**, 77 (1984); M. T. Ciotti, D. Mercanti, and G. Levi, in *A Dissection and Tissue Culture Manual of the Nervous System,* edited by A. Shahar, J. De Vellis, A. Vernadakis, and B. Haber (Liss, New York, 1989), pp. 291 and 292.

[10] The uptake buffer composition was 139 m*M* sucrose, 57.5 m*M* NaCl, 5 m*M* KCl, 2 m*M* $MgCl_2$, 1 mM $CaCl_2$, 12 m*M* glucose, 10 m*M* HEPES with a pH of 7.2. The final pH of the buffer was 7.5.

[11] R. M. Pruss, R. L. Akeson, M. M. Racke, and J. L. Wilburn, Neuron **7**, 509 (1991); Gelsomina De Stasio, P. Perfetti, N. Oddo, P. Galli, Delio Mercanti, M. Teresa Ciotti, S. F. Koranda, S. Hardcastle, B. P. Tonner, and G. Margaritondo, NeuroReport **3**, 965 (1992).

[12] R. M. Barnes, Chemia Analityczna **28**, 179 (1983); S. Caroli, E. Coni, A. Alimonti, E. Beccaloni, E. Sabbioni and R. Pietra, Analusis **16**, 75 (1988); L. Bourrier-Guerin, Y. Mauras, J. L. Truelle, and P. Allain, Trace Element in Medicine **2**, 88 (1985); C. De Martino, S. Caroli, A. Alimonti, F. Petrucci, G. Citro, and A. Nista, J. Exp. Clin. Cancer Res. **10**, 1 (1991).

[13] B. P. Tonner and G. R. Harp, J. Vac. Sci. Technol. **7**, 1 (1989).

[14] J. Stohr and R. Jaeger, Phys. Rev. B **26**, 4111 (1982); W. Wurth, J. Stohr, P. Feulner, X. Pan, K. R. Bauchspeiss, Y. Baba, E. Hudel, G. Rocker, and D. Menzel, Phys. Rev. Lett. **65**, 2426 (1990); Y. Ma, C. T. Chen, G. Meigs, K. Randall, and F. Sette, Phys. Rev. A **44**, 1848 (1991).

[15] A. LeFurgey, S. D. Davilla, D. A. Kopf, J. R. Sommer, and P. Ingram, J. Microsc. **165**, 191 (1992); D. E. Johnson, Ann. N.Y. Acad. Sci. **483**, 241 (1986); R. Rick, A. Dörge, F. X. Beck, and K. Thurau, *ibid.* **483**, 245 (1986); S. B. Andrews and T. S. Reese, *ibid.* **483**, 284 (1986).

[16] F. P. Ottensmeyer, Ann. N.Y. Acad. Sci. **483**, 339 (1986); H. Shuman, C. F. Chang, E. L. Buhle, Jr., and A. P. Somlyo, *ibid.* **483**, 295 (1986); C. Colliex *ibid.* **483**, 311 (1986); R. D. Leapman, *ibid.* **483**, 326 (1986).

[17] C. U. Ro, I. H. Musselman, and R. W. Linton, Ann. Chim. Acta **243**, 139 (1991); L. Vanvaeck, J. Bennett, W. Lauwers, A. Vertes, and R. Gijbels, Mikrochim. Acta **3**, 283 (1990); P. F. Schmidt and R. H. Barkhaus, Prog. Hystochem. Cytochem. **23**, 342 (1991).

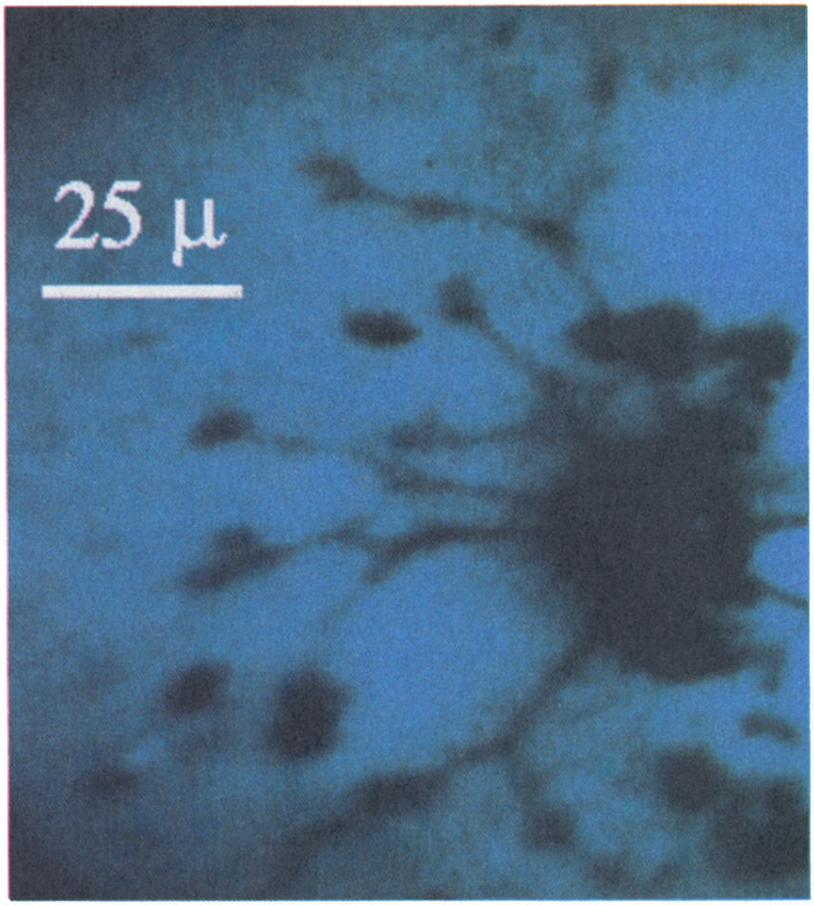

FIG. 1. XSEM secondary-photoelectron micrograph of a portion of neuron network of rat cultured cerebellar granule cells, taken with unmonochromated synchrotron light with a lateral resolution of the order of 0.5 μm. In the right-hand part of the image there is an aggregate of neurons, with several individual cells and their connections. In the central upper part, we see a growth cone.